Pflugers Arch - Eur J Physiol (2008) 457:233–242
DOI 10.1007/s00424-008-0497-2

INSTRUMENTS AND TECHNIQUES

A genetically encoded ratiometric sensor to measure extracellular pH in microdomains bounded by basolateral membranes of epithelial cells

Javier Urra · Moisés Sandoval · Isabel Cornejo · L. Felipe Barros · Francisco V. Sepúlveda · L. Pablo Cid

Received: 28 January 2008 / Revised: 3 March 2008 / Accepted: 17 March 2008 / Published online: 22 April 2008

Abstract Extracellular pH, especially in relatively inaccessible microdomains between cells, affects transport membrane protein activity and might have an intercellular signaling role. We have developed a genetically encoded extracellular pH sensor capable of detecting pH changes in basolateral spaces of epithelial cells. It consists of a chimerical membrane protein displaying concatenated enhanced variants of cyan fluorescence protein (ECFP) and yellow fluorescence protein (EYFP) at the external aspect of the cell surface. The construct, termed pHCECSensor01, was targeted to basolateral membranes of Madin–Darby canine kidney (MDCK) cells by means of a sequence derived from the aquaporin AQP4. The fusion of pH-sensitive EYFP with pH-insensitive ECFP allows ratiometric pH measurements. The titration curve of pHCECSensor01 in vivo had a pK_a value of 6.5± 0.04. Only minor effects of extracellular chloride on pHCECSensor01 were observed around the physiological concentrations of this anion. In MDCK cells, the sensor was able to detect changes in pH secondary to H^+ efflux into the basolateral spaces elicited by an ammonium prepulse or lactate load. This genetically encoded sensor has the potential to serve as a noninvasive tool for monitoring changes in extracellular pH microdomains in epithelial and other tissues in vivo.

Keywords pH sensor · Extracellular pH · Basolateral microdomains · MDCK cells · Ratiometric imaging · ECFP · EYFP · FRET

Both Javier Urra and Moisés Sandoval contributed equally to this work.

Electronic supplementary material The online version of this article (doi:10.1007/s00424-008-0497-2) contains supplementary material, which is available to authorized users.

J. Urra · M. Sandoval · I. Cornejo · L. F. Barros · F. V. Sepúlveda · L. P. Cid (✉)
Centro de Estudios Científicos (CECS),
Av. Arturo Prat 514,
Valdivia, Chile
e-mail: pcid@cecs.cl

L. F. Barros · F. V. Sepúlveda
CIN (Centro de Ingeniería de la Innovación del CECS),
Av. Arturo Prat 514,
Valdivia, Chile

The physiological importance of intracellular pH (pH_i) and its regulation have been well documented [33]. Cellular processes such as proliferation, differentiation, cell cycle progress, cell migration, and apoptosis all depend upon changes in pH_i. Much less attention has been given, however, to extracellular pH (pH_o), in particular that of relatively inaccessible compartments or domains that occur between cells in tissues. Several reports have stressed the importance of changes in the pH in these domains due to the pH dependence of the activity the membrane proteins such as receptors, transporters, ion channels, and enzymes. In the brain, pH transients occur in neurons, glial cells, and extracellular spaces in response to neuronal stimulation, to neurotransmitters and hormones as well as secondary to metabolic activity and ionic membrane transport [7]. In addition, a local change in pH_o at the interface between astrocytes' end-feet and capillaries could be a signal connecting neuronal activity and blood flow [31]. In the retina, pH_o in the vicinity of photoreceptors changes depending on the light stimulation, and it may have profound effects on neurotransmission and visual processing due to the pH sensitivity of ion channels [13, 22]. Moreover, the regulation of pH in narrow extracellular clefts in blood–organ barriers has been hypothesized to be critical for the survival of germ cells and photoreceptors [5].

It has been postulated that epithelial cells may be surrounded by a distinct pH_o at the apical surface, lateral intercellular spaces, and basal surface where it is different from the bulk medium [6, 8, 10, 19, 27, 32]. These pH microdomains are mainly related with epithelial transport activity, but they also affect the activity of the locally expressed transporters and channels. In small intestine, an acid microclimate has been measured adjacent to the apical surface which might be involved in the H^+-coupled transport of nutrients, micronutrients, and drugs [37]. In the colon, the absorption of short chain fatty acids coupled with sodium is thought to produce an acidification of the lateral intercellular spaces [9, 27, 29].

Investigators have hypothesized that rapid and local pH transients, and their effects on cellular processes, might be part of intra- and intercellular signaling cascades in nervous systems as well as in other tissues [11]. Understanding the physiological or pathological significance of these changes requires monitoring pH_o in real time with high spatial and temporal resolution. There are evident limitations in the experimental approaches available to study variations in the H^+ concentration in these micro- or nanodomains. An improvement in the space resolution without major disturbances in the tissue structure can be achieved, taking advantages of genetically encoded pH sensors based on green fluorescent protein (GFP) mutants.

The presence of a titrable group in the GFP chromophore makes these proteins suitable for the implementation of fluorescence-based pH indicators [14, 38]. Several studies have demonstrated the possibility of utilizing the yellow fluorescence protein (EYFP) variant to report intracellular pH [4, 18, 23, 25, 28, 35, 40], and the use of recombinant DNA technology has made it possible to target these proteins to specific subcellular compartments [25]. Another improvement has been achieved by the concatenation of two fluorescent proteins with different sensitivities to pH, thus gaining two advantages: generation of a ratiometric pH indicator and the possibility of using single-excitation dual-emission mode exploiting the energy transfer from cyan fluorescence protein (ECFP) to EYFP [1]. Furthermore, improvement in fluorescence resonance energy transfer (FRET) efficiency has been reported, truncating the C and N terminals of ECFP and EYFP, respectively [36].

The purpose of this study was to obtain a pH sensor capable of detecting pH variations in extracellular regions close to the cellular membrane. We generated an expression vector coding a fusion protein containing ECFP and EYFP displayed at the extracellular aspect of a transmembrane protein targeted to the basolateral membrane of epithelial cells. The sensor was able to detect local pH microdomains generated by proton extrusion through membrane transporters. This noninvasive tool can be useful to explore the role of extracellular pH in epithelia and other tissues.

Materials and methods

Plasmid construction

The backbone of pHCECSsensor01 is the mammalian expression vector pDisplay™ (Invitrogen) which contains the human cytomegalovirus (CMV) immediate-early promoter/enhancer, a leader sequence from murine Ig-κ chain, the sequence of the platelet-derived growth factor receptor transmembrane domain (PDGFR-TM) and the bovine growth hormone polyadenylation signal. The coding regions of the enhanced ECFP and EYFP were polymerase chain reaction (PCR) amplified from pEECFP-N1™ and pEEYFP-N1™ (Clontech) using primers that introduced restriction sites to clone them in tandem in pDisplay in frame upstream of the PDGFR-TM as follows. *Apa*I restriction sites were introduced in the sense and the antisense primers used to amplify ECFP (sense 5′-GGG CCC TCA TGG TGA GCA AGG GCG AGG AG-3′ and antisense 5′-GGG CCC CCT TGT ACA GCT CGT CCA T-3′). Similarly, a *Sma*I site was introduced in the sense and a *Sal*I site in the antisense primer used to amplify EYFP (sense 5′-CCC GGG ATG GTG ACG AAG GGC GAG GAG CTG-3′ and antisense 5′-GTC GAC CTT GTA CAG CTC GTC CAT GCC-3′). The coding sequence of the last 42 amino acids of the rat Aquaporin-4 (GenBank accession number U14007) was PCR amplified introducing a *Not*I in the sense primer and a *Xho*I in the antisense primer which were used to insert it in frame downstream of the PDGFR-TM (sense 5′-GCG GCC GCA GAC AAC CGG AGC CAA GTG G-3′ and antisense 5′-CTC GAC TCA TAC AGA AGA TAA TAC C-3′).

Stable cell line generation and characterization

Madin–Darby canine kidney (MDCK-1) cells were grown at 37°C in modified Eagle's medium (MEM) supplemented with 10% of fetal bovine serum in an atmosphere of 5% CO_2. To establish the MDCK pHCECSensor01 cell line, 50% confluent cells were transfected with 5 μg of the construct using Lipofectamine (Invitrogen) following the manufacturer instructions. After 3 h, the cells were washed and maintained in MEM supplemented with 10% of fetal bovine serum and 1 mg/ml geneticin (Gibco). The selection media was changed every 3 days. After 10 days, resistant colonies were isolated using plastic cylinders. The selection criterion was the expression of the sensor protein in the cell membrane assessed by fluorescence microscopy.

Immunoblot analysis of total protein extracts was done as described previously [15]. Antibodies (1:5,000) used were anti-HA (rat monoclonal clone 3F10, Roche), Anti-*myc* (mouse monoclonal clone 9E10, Sigma), and anti-GFP (rabbit polyclonal anti-GFP, Molecular Probes). Secondary HRP-conjugated antibodies (Jackson) were used at 1:50,000.

Optical measurements

Spectral analysis was done using a Perkin Elmer LS55 luminescence spectrometer. Emission spectra were collected at 430±3-nm excitation between 450 and 600 nm (6-nm slit). Cell extracts were obtained by lysing subconfluent cultures with a buffer of the following composition: 1% Triton X-100, 90 mM NaCl, 50 mM Na gluconate, 50 mM MES pH 5.5. Proteases were inhibited using 5 mM ethylenediaminetetraacetic acid, 500 μM phenylmethanesulphonyl fluoride, 10 μg/ml aprotinin, 10 μM leupeptin, and 1 μg/ml pepstatin A. After obtaining the spectrum at pH 5.5, the cell extract was alkalinized to pH 8.6 by addition of NaOH. The spectra of pHCECSensor01 were obtained after subtraction of the parental MDCK cell spectra obtained with the same amount of protein.

Confocal imaging was carried out with a LSM 5 Pascal Zeiss confocal microscope, either with a 63×, 1.2 NA (numerical aperture) water immersion objective or a 40×, 1.3 NA oil immersion objective. Both the sensor and calcein were imaged at 488-nm excitation and 505- to 550-nm emission. In the X mode (lines of 512 pixels) and in the XY mode (frames of 512×512 pixels), pinhole was adjusted to obtain optical sections <1.3 μm. In the XYZ mode (frames of 1,024×1,024 pixels collected every 0.5 μm), pinhole was set to give 1.3 Airy units. Z-stacks were processed using Huygens Essential deconvolution software (Scientific Volume Imaging, The Netherlands).

Ratiometric fluorescence imaging was carried out using an inverted Olympus IX-70 microscope equipped with a 63×1.4 NA oil immersion objective, an Optoscan monochromator, an Optosplit image splitter (Cairn, Faversham, UK), and a Hamamatsu Orca CCD camera (Hamamatsu City, Japan) under the control of Kinetic Imaging Image Acquisition Software (AQM Advance-6). Cultures were excited at 430 nm and emission was collected at 485 and 535 nm. The imaging was performed using an excitation beamsplitter dichroic (51017bs), an emission long-pass dichroic (515dclp), and two emission filters (D485/40 for ECFP and D535/30 for EYFP; all from Chroma Technology, Brattleboro, VT, USA). Regions of interest (ROIs) were selected for quantitation purposes.

pH measurements

All experiments were carried out at room temperature (22–24°C) with the MDCK cell line grown on glass coverslips. Before the experiments, cells were incubated with 10 mM sodium butyrate for 24 h and then superfused using a standard solution of the following composition in mM: 90 NaCl, 45 Na gluconate, 5 KCl, 2 $CaCl_2$, 1 $MgCl_2$, and 10 HEPES, pH 7.4. The osmolality was adjusted to 300 mOsm/l with sucrose. Calibration solutions were prepared using a standard solution buffered with 10 mM of the following the buffers: MES for pH 5.5, 6.0, and 6.5 solutions, HEPES for pH 7.0, 7.5, and 8.0 solutions, AMPSO for pH 8.5 and 9.0 solutions. In Na^+-free solutions, NaCl was equimolarly replaced by *N*-metyl-D-glucamine (NMDG) chloride. In lactate load experiments, bicarbonate buffer was used, in mM: Na gluconate 80, Na bicarbonate 25, KH_2PO_4 3.3, K_2HPO_4 0.8, and $CaCl_2$ 1.2 and were equilibrated with 5% CO_2/air. In lactate-containing solution, 25 mM Na lactate replaced an equivalent amount of Na gluconate. The osmolality was adjusted to 300 mOsm/l with sucrose. The inhibitor α-Cyano-4-hydroxycinnamate (Sigma) was added fresh to the buffer before the experiments. Ammonium prepulse technique [33] was carried out as follows: The cells were perfused during 5 min with standard solution where 25 mM of NH_4Cl replaced the same amount of NaCl or NMDG Cl.

Data analysis

Average fluorescence intensities from ROIs were obtained, corrected for background, and ratioed. All data are represented as means ± SEM. Experiments were repeated at least three times with similar results. Calibration curves were built by expressing fluorescence ratios (R=535:485) as function of proton concentration and normalized to value obtained at pH 7.4. pK_a values were obtained by nonlinear regression (SigmaPlot) using the following equation [17]:

$$R = R_0 + \left((R_{\max} - R_0) \times 10^{-\mathrm{p}K_a}\right) / \left(10^{-\mathrm{p}K_a} + [\mathrm{H}^+]\right) \quad (1)$$

where R_0 and $R_{\max}$ are extrapolated asymptotic values at low and high pH, respectively.

The effect of Cl^- concentration was also described using a single binding site model [21]. Confocal time series experiments were expressed as change in fluorescence intensity normalized to initial fluorescence ($\Delta F/F_0$).

Results

Vector construction

The pHCECSensor01 vector (see Fig. 1a) was constructed utilizing the pDisplay™ mammalian expression vector. Proteins expressed from pDisplay™ are normally fused at the N terminus to the murine Ig-κ chain leader sequence, which directs the protein to the secretory pathway. At the C terminus, the PDGFR transmembrane domain (TMD) anchors the protein to the plasma membrane displaying it on the extracellular side. To build up the pHCECSensor01 vector, the complementary DNAs (cDNAs) for EYFP and ECFP were engineered in tandem as the proteins to be displayed. The fluorophores were coupled via a nine amino

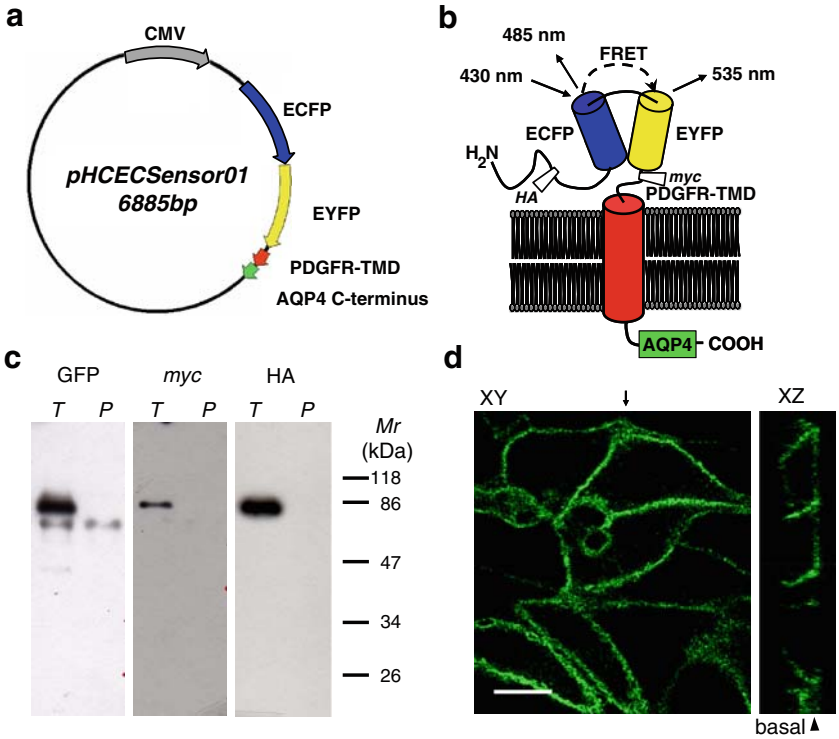

Fig. 1 Construction of the pHCECSensor01. **a** Vector assembled to produce the extracellular pH sensor is based on the pDisplay™ mammalian expression vector. Main elements, drawn schematically as *colored arrows*, are the coding sequences of the CMV promoter, the transmembrane domain of platelet-derived growth factor receptor (*PDGFR-TMD*), the enhanced forms of the yellow fluorescent protein (*EYFP*) and the cyan fluorescent protein (*ECFP*), and a C terminus domain of aquaporin AQP4. **b** Predicted topology of the pHCECSensor01 at the basolateral plasma membrane displaying EYFP and ECFP at the extracellular surface. A possible mechanism for fluorescence resonance energy transfer (*FRET*) between ECFP and EYFP is also shown. **c** Immunoblot of total protein from pHCECSensor01-expressing MDCK cells: The presence of sensor was probed with antibodies directed against GFP, *myc*, and HA epitopes. In each case, the same samples from the stably transfected (*T*) or parental (*P*) cells were run as indicated. **d** Polarized targeting of pHCECSensor01. MDCK cells stably expressing pHCECSensor01 were grown on glass coverslips and imaged by confocal microscopy. The *arrow* at the *top* of the XY image indicates where the YZ section was obtained. The *arrowhead* indicates the base of the monolayer. The calibration bar is 10 μm

acid linker (G-A-Q-P-A-R-S-P-G). The cDNA encoding the last 42 amino acid C terminus of the aquaporin AQP4 was subcloned as shown in Fig. 1a. Expression of the resulting vector in mammalian cells is predicted to produce the membrane protein schematized in Fig. 1b: a protein anchored to the membrane by the TMD of PDGFR displaying EYFP and ECFP at the extracellular surface. If the cells used were polarized epithelial cells, the AQP4 C terminus is expected to circumscribe that expression to the basolateral membranes [26]. The necessity for a basolateral targeting sequence was established in preliminary experiments where a pDisplay-EYFP construct without the AQP4 motif was expressed in a non-polarized manner in MDCK cells (not shown).

Expression of pHCECSensor01 in MDCK cells

An MDCK cell line stably expressing pHCECSensor01 was generated and used in the following experiments. Expression of pHCECSensor01 in the cell line was first examined by immunoblot of total protein. We took advantage of the presence of a Hemagglutinin A (HA) epitope tag towards the N-terminal end of the construct and a *myc* epitope located immediately extracellular to the PDGFR TMD (see Fig. 1b). Figure 1c shows immunoblots obtained with anti-HA and anti-myc antibodies. In addition, an anti-GFP antibody was used that should recognize both ECFP and EYFP. A single band was observed in the HA and *myc* immunoblots made on protein from the pHCECSensor01 cell line (T) with a molecular mass consistent with that expected for the complete construct (70 kDa). This band was absent from the parental cell line (P). The immunoblot done with anti-GFP antibody also revealed a predominant band of around 70 kDa which was absent from the parental cells. A second band of lower apparent molecular mass was also present in the parental cell line, suggesting it was due to non-specific staining. Anti-GFP also revealed a faint band observed only in the sensor-transfected cells at around 47-kDa molecular mass. Concerning the subcellular localization of pHCECSensor01, confocal microscopy (Fig. 1d) of the sensor-expressing cell line showed the highest fluorescence at the borders between cells, consistent with

basolateral surface expression. The basolateral membrane expression is also confirmed in the XZ section shown in Fig. 1d. There was also fluorescence inside the cells.

To test whether the cell line was capable of building intercellular microdomains, cultures were pre-equilibrated with calcein, a water-soluble fluorophore that stains the extracellular space. Upon calcein washout, the dye present in intercellular clefts disappeared slowly (Fig. 2), evidencing a diffusional restriction. The restriction was strongly determined by the degree of culture confluency, with halftimes ranging from seconds at low confluency (Fig. 2a) to several minutes in packed monolayers (Fig. 2c).

pH-sensitivity of pHCECSensor01

Figure 3a shows emission spectra for pHCECSensor01 excited at 430 nm. At alkaline pH, two peaks were observed consistent with emission maxima of ECFP and EYFP, showing the presence of FRET. Acidification to pH 5.5 eliminated the second peak consistent with a marked quenching of EYFP fluorescence. As there was no apparent change in the blue peak, it can be surmised that FRET efficiency was not affected by pH. The graph also indicates the emission windows that were selected to perform imaging experiments with intact cells. An example of such cells exhibiting pHCECSensor01 fluorescence is shown Fig. 3b, which presents the subcellular distribution of the sensor as imaged at the two emission windows. The experiment in Fig. 3c confirms that EYFP emission is much more sensitive to pH [25], making the ratio between EYFP and ECFP emission a pH readout that is not affected by sensor concentration. Titration of the sensor in cultures at 60–70% confluency gave a pK_a value parameter that was not significantly different from that obtained at lower than

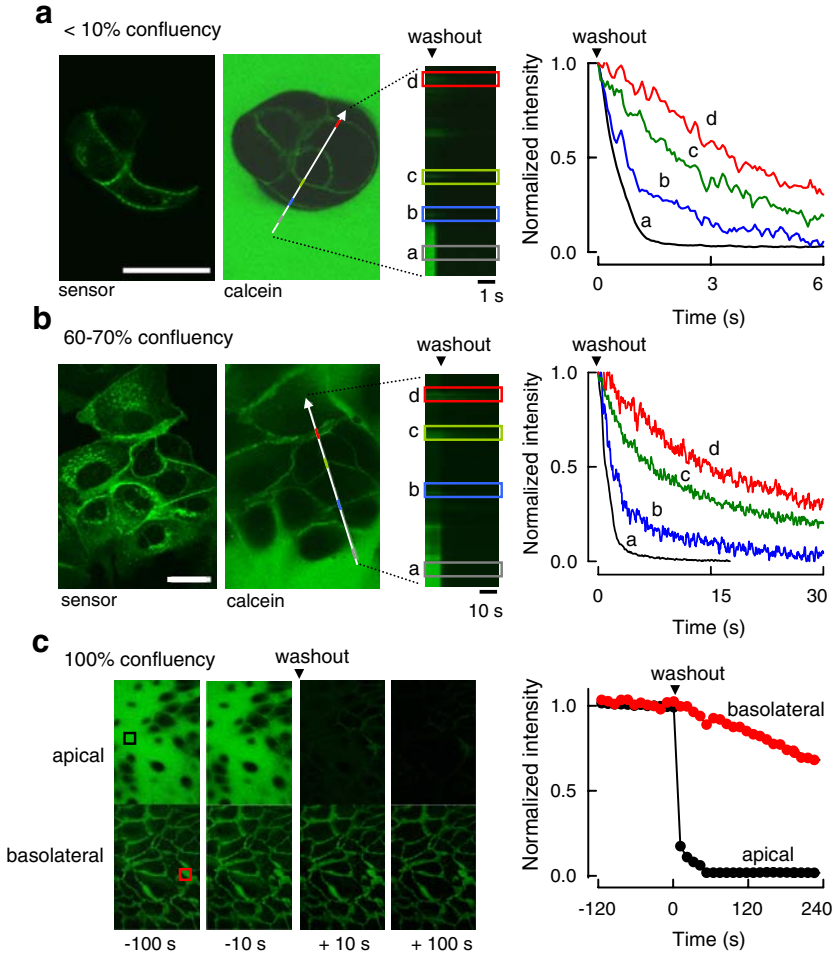

Fig. 2 Diffusion-restricted basolateral compartments in MDCK cultures. Confocal images were first obtained to register the location of the sensor. After 95% reduction of laser power, at which the sensor was not detectable, the extracellular space was stained with 50 μM calcein. The effect of dye washout was then measured. **a** Fluorescence was recorded in a low confluency culture every 40 ms along the *white arrow* (linescan image). Average intensities in four regions selected in the linescan (*1*, *2*, *3*, *4*) are plotted on the *right panel*. **b** A similar experiment performed in a more confluent culture. **c** A post-confluent culture was imaged every 10 s just above the monolayer (apical) and inside the monolayer (basolateral). The *panel* on the *right* shows the average fluorescence intensities of the ROIs plotted on the left panel. Bars are 25 μm

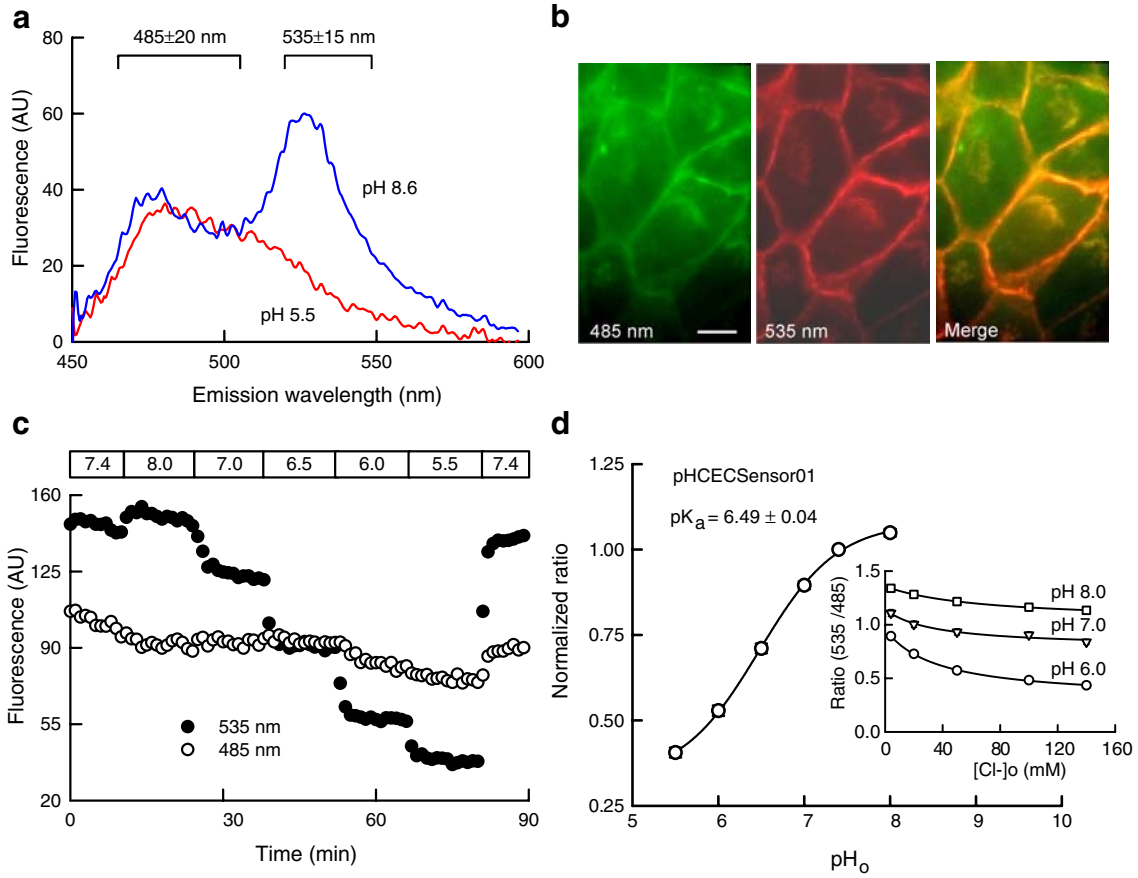

Fig. 3 pH sensitivity of pHCECSensor01. **a** Emission spectra of pHCECSensor01 obtained using a cell extract at pH 5.5 and after alkalinizing to pH 8.6. Fluorescence was corrected for background spectra obtained in a similar manner with a parental cell extract. The windows used in the fluorescence ratio experiments are indicated. **b** Cell images taken in the dual fluorescence emission microscope. Cells were exposed to 430 nm, and the emission was imaged at both 485 and 535 nm. Bar is 10 μm. **c** Representative time course experiment showing the response of sensor fluorescence to changes in extracellular pH. **d** Ratios were calculated between fluorescence emissions at 535 and 485 nm and then normalized relative to the value at pH 7.4 (mean ± SEM, for 26 ROIs in seven separate experiments). The *line* shows the best fit of Eq. 1 to the data. The *inset* shows the effect of $[Cl^-]_o$ upon pHCECSensor01 fluorescence at three different pH_o values (means ± SEM, n=4–7 ROIs)

10% confluency, suggesting that under basal conditions, MDCK cells do not generate significant standing pH microdomains. Accordingly, all the titration experiments were pooled together as illustrated in Fig. 3d, giving a pK_a of 6.5. This was used to convert ratios into pH values.

A possible factor affecting the pH measurement with pHCECSensor01 is the surface potential of the plasma membrane [20]. We think this unlikely, as experiments with EYFP tethered to the outside of the membrane surface with the pDisplay system gave the same results as those for EYFP free in solution. Our results (see Supplementary Fig. 2) gave a pK_a value of 7.07 and a Hill coefficient of 1.08 for membrane-tethered EYFP, which compare with a pK_a value of 7.1 and a Hill coefficient of 1.1 for EYFP in solution [25].

EYFP fluorescence is sensitive to Cl^- [21, 24, 41]. As expected, pHCECSensor01 display a significant sensitivity to Cl^- (see Supplementary Fig. 1) that would make its use difficult in the presence of important Cl^- concentration changes. Fortunately, the sensitivity of the sensor to Cl^- had a half saturation value of about 30 mM at pH 6.0 and 35 mM at pH 7.0 and therefore near saturation at physiological extracellular chloride concentrations (inset to Fig. 3d). This means that its use as a pH sensor at typical extracellular Cl^- concentrations will not be affected by small shifts in the concentration of the anion. These putative spontaneous changes in $[Cl^-]_o$ are, at any rate, unlikely to arise from channel- or carrier-mediated Cl^- flux [2].

Basolateral intercellular spaces as pH-microclimate domains

Having ascertained the capacity of pHCECSensor01 to sense extracellular pH and its basolateral targeting in polarized epithelial cell monolayers, we proceeded to explore the possibility that diffusion-restricted spaces bounded by basolateral membranes could constitute a pH microdomain under conditions of increased proton efflux.

We used two maneuvers to increase proton efflux into the basolateral spaces. The first consisted in an NH_4^+ load, which is widely used to produce an intracellular acidification [33]. The intracellular pH is restored by the action of a Na^+/H^+ exchanger which pumps H^+ out of the cells across the basolateral membrane [39]. For these experiments, we chose cultures at 60–70% confluency because the sensor was calibrated at this confluency and diffusion into their basolateral spaces is partially restricted, allowing the access of the experimental solutions (Fig. 2). Figure 4a and b shows that after the NH_4^+ prepulse, the sensor detected a transient acidification of the basolateral space that was diminished by increasing the buffer capacity of the medium. Taking advantage of the small fraction of the sensor present in intracellular locations, we monitored both intracellular and extracellular pH using confocal microscopy. Figure 4c reveals that the ammonium prepulse caused the expected intracellular alkalinization due to proton capture by NH_3 [33]. Contrary to this, there was little change in the fluorescence recorded at extracellular locations. When NH_4^+ was removed in the absence of Na^+, the cells were unable to recover the intracellular pH and failed to acidify the basolateral clefts. Upon Na^+ reintroduction, a rapid intracellular alkalinization took place which coincided with

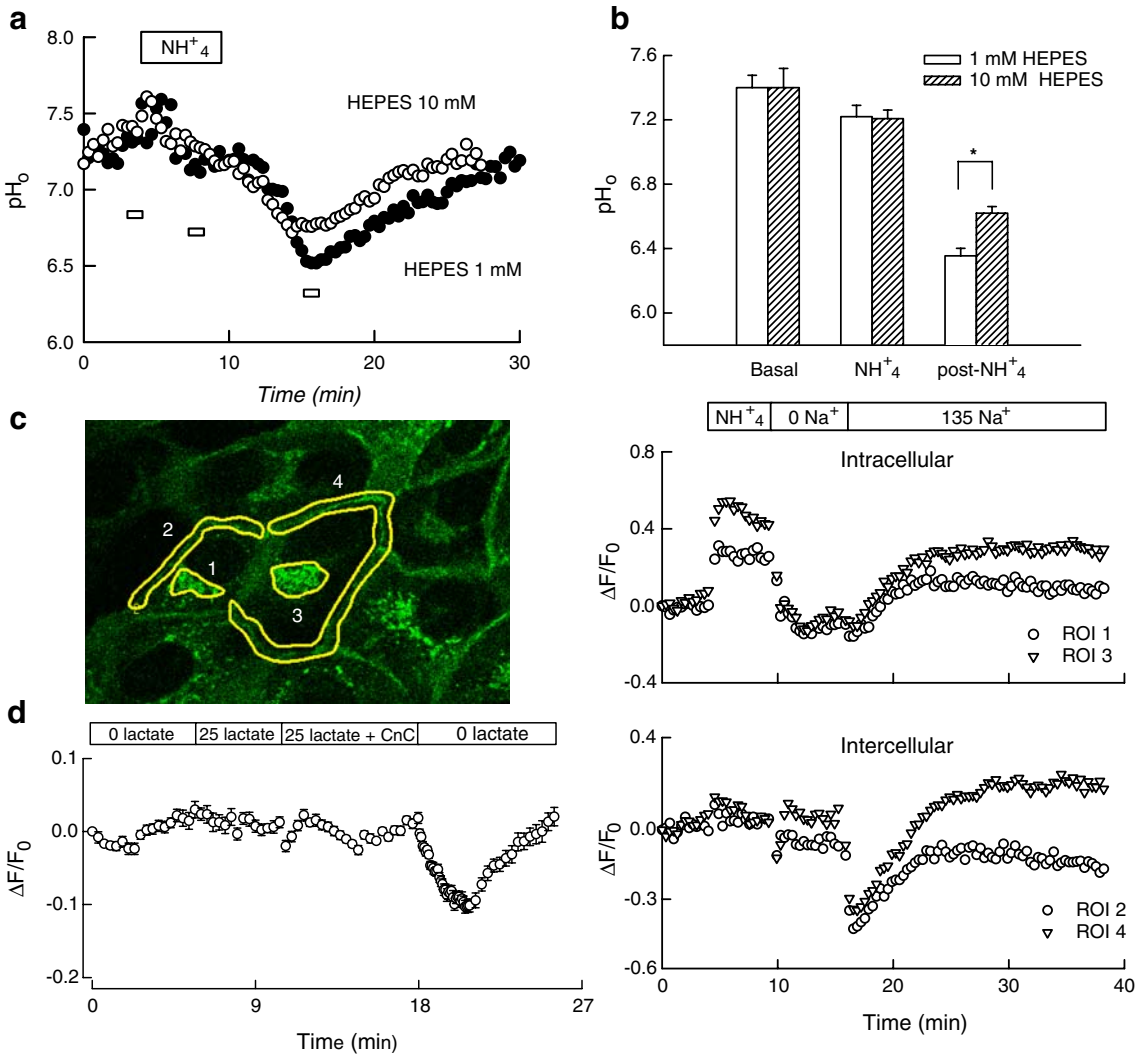

Fig. 4 Basolateral intercellular spaces as pH-microclimate domains. **a** Time course of a NH_4^+ load experiment in which the extracellular pH was determined using two buffer capacities. **b** The graph summarizes the pH data extracted from the times shown by the boxes in **a**. *Asterisk* indicates a significant difference ($p<0.05$) between measurements. **c** Confocal image of a NH_4^+ load experiment showing ROIs chosen for analysis. Plots on the *right* show the time course of the changes in fluorescence at intracellular (*above*) and intercellular (*bottom*) ROIs. The bathing solution was changed from a control 135 mM Na^+-containing solution to one free of Na^+ made by *N*-methyl-D-glucamine replacement. Ammonium load was effected by superfusion with 25 mM NH_4^+. This was followed by superfusion with NH_4^+ -free solutions containing 0 and then 135 mM Na^+ **d** The graph shows a lactate-load experiment. Cells were superfused with 25 mM lactate followed by removal of lactate, first in the presence of 5 mM α-cyanocinnamate (*CnC*) and then in CnC-free control solution. Means ± SEM for eight ROIs

an acidification of the basolateral clefts. The Na^+ dependency of this phenomenon is consistent with the participation of Na^+/H^+ exchangers.

A second maneuver to increase H^+ efflux into the basolateral spaces was to force the cells to export lactate via the monocarboxylate/H^+ cotransporters (MCTs). In MDCK cells, MCT1 is expressed basolaterally [12, 34] so that removal of extracellular lactate after loading should elicit a basolateral space acidification. Figure 4d shows that removal of extracellular lactate in the presence of α-Cyano-4-hydroxycinnamate (CnC), an inhibitor of MCT transporters, failed to affect basolateral pH. However, when washout of the CnC allowed the MCT function, there was a clear basolateral acidification, consistent with MCT-mediated exit of lactate into a pH microclimate domain.

Discussion

The pH in microdomains at the narrow extracellular clefts separating organs from the systemic circulation has been proposed to be an important determinant of tissue physiology and pathophysiology [5, 7, 42]. Extracellular protons could even serve as neurotransmitters as suggested by recent work on *Caenorhabditis elegans* where a proton receptor has been identified in muscle [3].

The existence of these potentially important functions of pH in extracellular spaces makes it necessary to develop means for quantitatively probing these pH microdomains in a noninvasive, time-resolved manner. Here, we have generated a genetically encoded, ratiometric sensor targeted to basolateral membranes of epithelia suitable for tackling some of these questions in live tissues.

The pHCECSensor01 was constructed to display the fluorophores ECFP and EYFP extracellularly using as a basis the pDisplay™ system, which anchors proteins to the membrane through fusion to a transmembrane domain from platelet derived growth factor receptor. Our addition of a C terminus targeting domain of the aquaporin AQP4 [26] ensured the basolateral expression of the construct in polarized epithelial cells as revealed by confocal microscopy of an MDCK cell line stably expressing pHCECSensor01. Expression of pHCECSensor01 in the cell line was stable, with very little degradation of the sensor as detected by immunoblot.

pHCECSensor01 was designed to obtain a ratiometric estimation of pH whether FRET between the ECFP and EYFP moieties of the sensor occurred or not. In addition to the expected blue peak corresponding to ECFP, exciting at 430 nm elicited a strong green peak corresponding to the known emission peak of EYFP. Because the magnitude of the blue peak was similar after acidification, we reckon that energy transfer is not pH-sensitive. The contrasting pH sensitivities of ECFP and EYFP [25] make the sensor a suitable ratiometric reporter of proton concentration.

In addition to its pH sensitivity, EYFP fluorescence is also sensitive to Cl^- [21, 24, 41]. This is a disadvantage if changes in the concentration of the anion are envisaged as part of the experimental protocol. As shown, however, saturation of the effect on the fluorescence ratio reported by the sensor occurs at physiological extracellular concentrations. As spontaneous changes in $[Cl^-]_o$ are unlikely to arise from channel- or carrier-mediated Cl^- flux into or from the extracellular spaces under consideration [2], an uncontrolled interference from the anion is not expected. Nevertheless, having proven the correct targeting of pHCECSensor01 to the desired membrane domains, other fluorophores less sensitive to Cl^- could be considered instead of EYFP. Mutational work on EYFP has produced rather Cl^--insensitive variants, which unfortunately also have decreased pH sensitivity [16, 30]. Measurements of pH in compartments subjected to important changes in Cl^- concentration will have to await the development of improved versions of EYFP.

Our experiments with pHCECSensor01 revealed diffusion-restricted spaces bounded by basolateral membranes that can constitute pH microdomains under conditions of increased proton efflux. These domains are generated by the activity of transporters that are also active under physiological conditions in transporting epithelia. Some examples are the basolateral spaces of proximal tubule cells during bicarbonate reabsorption in the kidney, lactate transport in blood tissue barriers in the testes and the retina, and short-chain fatty acid absorption in the colon. In the brain, protons and bicarbonate are quickly exchanged between neurons, astrocytes, and the extracellular space in response to changes in neuronal activity. In all these tissues, local extracellular pH domains are important regulators of cell function. The precise time-resolved quantification of pH of these domains will be crucial in our understanding of the role of extracellular protons as a signal.

Use of pH sensors that can be targeted in animals has the potential to explore pH microdomains in living tissues. The basic structure of the sensor described here is a good platform for modifications of the pH-sensing range and other desirable characteristics such as FRET efficiency and sensitivity to other physiological parameters.

Acknowledgments This work was supported by Fondecyt grant 1051081. The Centro de Estudios Científicos is funded by an Institute grant from the Millennium Science Initiative and by Centers of Excellence Base Financing Program, Conicyt and Gobierno Regional de Los Ríos. CECS is also supported by the following corporate benefactors: Antofagasta Minerals, Arauco, Empresas CMPC, Indura, Naviera Ultragas, and Telefónica del Sur. We are grateful to Dr. Jennifer Carbrey, Duke University Medical Center for providing the rat AQP4 plasmid, Dr. David Sheppard, University of Bristol for providing MDCK-1 cells, and Dr. Wolf Frommer, Carnegie Institution for kind donation of plasmids. The help of Gaspar Peña in the construction of the

perfusion chamber used in confocal studies is gratefully acknowledged. We are grateful to Dr. Rafael Burgos, Universidad Austral de Chile for generously providing access to equipment.

References

1. Awaji T, Hirasawa A, Shirakawa H, Tsujimoto G, Miyazaki S (2001) Novel green fluorescent protein-based ratiometric indicators for monitoring pH in defined intracellular microdomains. Biochem Biophys Res Commun 289:457–462
2. Barros LF, Martínez C (2007) An enquiry into metabolite domains. Biophys J 92:3878–3884
3. Beg AA, Ernstrom GG, Nix P, Davis MW, Jorgensen EM (2008) Protons act as a transmitter for muscle contraction in *C. elegans*. Cell 132:149–160
4. Bizzarri R, Arcangeli C, Arosio D, Ricci F, Faraci P, Cardarelli F, Beltram F (2006) Development of a novel GFP-based ratiometric excitation and emission pH indicator for intracellular studies. Biophys J 90:3300–3314
5. Bosl MR, Stein V, Hubner C, Zdebik AA, Jordt SE, Mukhopadhyay AK, Davidoff MS, Holstein AF, Jentsch TJ (2001) Male germ cells and photoreceptors, both dependent on close cell–cell interactions, degenerate upon ClC-2 Cl^- channel disruption. EMBO J 20:1289–1299
6. Chatton JY, Spring KR (1994) Acidic pH of the lateral intercellular spaces of MDCK cells cultured on permeable supports. J Membr Biol 140:89–99
7. Chesler M (2003) Regulation and modulation of pH in the brain. Physiol Rev 83:1183–1221
8. Chu S, Montrose MH (1995) Extracellular pH regulation in microdomains of colonic crypts: effects of short-chain fatty acids. Proc Natl Acad Sci USA 92:3303–3307
9. Chu S, Montrose MH (1997) Transepithelial SCFA fluxes link intracellular and extracellular pH regulation of mouse colonocytes. Comp Biochem Physiol A Physiol 118:403–405
10. Chu S, Tanaka S, Kaunitz JD, Montrose MH (1999) Dynamic regulation of gastric surface pH by luminal pH. J Clin Invest 103:605–612
11. Deitmer JW, Rose CR (1996) pH regulation and proton signalling by glial cells. Prog Neurobiol 48:73–103
12. Deora AA, Philp N, Hu J, Bok D, Rodriguez-Boulan E (2005) Mechanisms regulating tissue-specific polarity of monocarboxylate transporters and their chaperone CD147 in kidney and retinal epithelia. Proc Natl Acad Sci USA 102:16245–16250
13. Dmitriev AV, Mangel SC (2001) Circadian clock regulation of pH in the rabbit retina. J Neurosci 21:2897–2902
14. Elsliger MA, Wachter RM, Hanson GT, Kallio K, Remington SJ (1999) Structural and spectral response of green fluorescent protein variants to changes in pH. Biochemistry 38:5296–5301
15. Gallardo P, Cid LP, Vio CP, Sepúlveda FV (2001) Aquaporin-2, a regulated water channel, is expressed in apical membranes of rat distal colon epithelium. Am J Physiol 281:G856–G863
16. Griesbeck O, Baird GS, Campbell RE, Zacharias DA, Tsien RY (2001) Reducing the environmental sensitivity of yellow fluorescent protein. Mechanism and applications. J Biol Chem 276:29188–29194
17. Grynkiewicz G, Poenie M, Tsien RY (1985) A new generation of Ca^{2+} indicators with greatly improved fluorescence properties. J Biol Chem 260:3440–3450
18. Hanson GT, McAnaney TB, Park ES, Rendell ME, Yarbrough DK, Chu S, Xi L, Boxer SG, Montrose MH, Remington SJ (2002) Green fluorescent protein variants as ratiometric dual emission pH sensors. 1. Structural characterization and preliminary application. Biochemistry 41:15477–15488
19. Harris PJ, Chatton JY, Tran PH, Bungay PM, Spring KR (1994) pH, morphology, and diffusion in lateral intercellular spaces of epithelial cell monolayers. Am J Physiol 266:C73–C80
20. Heberle J, Dencher NA (1992) Surface-bound optical probes monitor protein translocation and surface potential changes during the bacteriorhodopsin photocycle. Proc Natl Acad Sci USA 89:5996–6000
21. Jayaraman S, Haggie P, Wachter RM, Remington SJ, Verkman AS (2000) Mechanism and cellular applications of a green fluorescent protein-based halide sensor. J Biol Chem 275:6047–6050
22. Jonz MG, Barnes S (2007) Proton modulation of ion channels in isolated horizontal cells of the goldfish retina. J Physiol 581:529–541
23. Kneen M, Farinas J, Li Y, Verkman AS (1998) Green fluorescent protein as a noninvasive intracellular pH indicator. Biophys J 74:1591–1599
24. Kuner T, Augustine GJ (2000) A genetically encoded ratiometric indicator for chloride: capturing chloride transients in cultured hippocampal neurons. Neuron 27:447–459
25. Llopis J, McCaffery JM, Miyawaki A, Farquhar MG, Tsien RY (1998) Measurement of cytosolic, mitochondrial, and Golgi pH in single living cells with green fluorescent proteins. Proc Natl Acad Sci USA 95:6803–6808
26. Madrid R, Le Maout S, Barrault MB, Janvier K, Benichou S, Merot J (2001) Polarized trafficking and surface expression of the AQP4 water channel are coordinated by serial and regulated interactions with different clathrin-adaptor complexes. EMBO J 20:7008–7021
27. Maouyo D, Chu S, Montrose MH (2000) pH heterogeneity at intracellular and extracellular plasma membrane sites in HT29-C1 cell monolayers. Am J Physiol Cell Physiol 278:C973–C981
28. Miesenbock G, De Angelis DA, Rothman JE (1998) Visualizing secretion and synaptic transmission with pH-sensitive green fluorescent proteins. Nature 394:192–195
29. Montrose MH, Chu S (1997) Transepithelial SCFA gradients regulate polarized Na/H exchangers and pH microdomains in colonic epithelia. Comp Biochem Physiol A Physiol 118:389–393
30. Nagai T, Ibata K, Park ES, Kubota M, Mikoshiba K, Miyawaki A (2002) A variant of yellow fluorescent protein with fast and efficient maturation for cell-biological applications. Nat Biotechnol 20:87–90
31. Newman EA (1996) Acid efflux from retinal glial cells generated by sodium bicarbonate cotransport. J Neurosci 16:159–168
32. Rechkemmer G, Wahl M, Kuschinsky W, von Engelhardt W (1986) pH-microclimate at the luminal surface of the intestinal mucosa of guinea pig and rat. Pflugers Arch 407:33–40
33. Roos A, Boron WF (1981) Intracellular pH. Physiol Rev 61:296–434
34. Rosenberg SO, Fadil T, Schuster VL (1993) A basolateral lactate/H^+ co-transporter in Madin–Darby canine kidney (MDCK) cells. Biochem J 289:263–268
35. Sankaranarayanan S, De Angelis D, Rothman JE, Ryan TA (2000) The use of pHluorins for optical measurements of presynaptic activity. Biophys J 79:2199–2208
36. Shimozono S, Hosoi H, Mizuno H, Fukano T, Tahara T, Miyawaki A (2006) Concatenation of cyan and yellow fluorescent proteins for efficient resonance energy transfer. Biochemistry 45:6267–6271
37. Thwaites DT, Anderson CM (2007) H^+-coupled nutrient, micronutrient and drug transporters in the mammalian small intestine. Exp Physiol 92:603–619
38. Tsien RY (1998) The green fluorescent protein. Annu Rev Biochem 67:509–544
39. Vilella S, Guerra L, Helmle-Kolb C, Murer H (1992) Characterization of basolateral Na/H exchange (Na/H-1) in MDCK cells. Pflugers Arch 420:275–280
40. Wachter RM, King BA, Heim R, Kallio K, Tsien RY, Boxer SG, Remington SJ (1997) Crystal structure and photodynamic behavior

of the blue emission variant Y66H/Y145F of green fluorescent protein. Biochemistry 36:9759–9765
41. Wachter RM, Yarbrough D, Kallio K, Remington SJ (2000) Crystallographic and energetic analysis of binding of selected anions to the yellow variants of green fluorescent protein. J Mol Biol 301:157–171
42. Warth R, Barrière H, Meneton P, Bloch M, Thomas J, Tauc M, Heitzmann D, Romeo E, Verrey F, Mengual R, Guy N, Bendahhou S, Lesage F, Poujeol P, Barhanin J (2004) Proximal renal tubular acidosis in TASK2 K^+ channel-deficient mice reveals a mechanism for stabilizing bicarbonate transport. Proc Natl Acad Sci USA 101:8215–8220